

New Generation of Climate Models Track Recent Unprecedented Changes in Earth's Radiation Budget Observed by CERES

1 Norman G. Loeb^{1*}, Hailan Wang², Richard Allan³, Timothy Andrews⁴, Kyle Armour⁵,
2 Jason N.S. Cole⁶, Jean-Louis Dufresne⁷, Piers Forster⁸, Andrew Gettelman⁹, Huan Guo¹⁰,
3 Thorsten Mauritsen¹¹, Yi Ming¹⁰, David Paynter¹⁰, Cristian Proistosescu^{12,13}, Malte F.
4 Stuecker¹⁴, Ulrika Willén¹⁵, Klaus Wyser¹⁵

5 ¹NASA Langley Research Center, Hampton, VA, USA

6 ²Science Systems and Applications, Inc., Hampton, Virginia, USA

7 ³Department of Meteorology and National Centre for Earth Observation, University of
8 Reading, Reading, UK

9 ⁴Met Office Hadley Centre, Exeter, UK

10 ⁵Department of Atmospheric Sciences, University of Washington, Seattle, WA, USA

11 ⁶Canadian Centre for Climate Modelling and Analysis, Environment and Climate Change
12 Canada, Victoria, BC, Canada

13 ⁷Laboratoire de Météorologie Dynamique, Institut Pierre et Simon Laplace, Paris, France

14 ⁸School of Earth and Environment, University of Leeds, Leeds, UK

15 ⁹National Center for Atmospheric Research, Boulder, CO, USA

16 ¹⁰NOAA/Geophysical Fluid Dynamics Laboratory, Princeton University, Princeton, NJ,
17 USA

18 ¹¹Department of Meteorology, Stockholm University, Stockholm, Sweden

19 ¹²Joint Institute for the Study of the Atmosphere and Ocean, University of Washington,
20 Seattle, WA, USA

21 ¹³Departments of Atmospheric Sciences and Geology, University of Illinois Urbana-
22 Champaign, IL, USA

23 ¹⁴Department of Oceanography and International Pacific Research Center, School of
24 Ocean and Earth Science and Technology, University of Hawai'i at Mānoa, Honolulu,
25 HI, USA

26 ¹⁵Rosby Centre, Swedish Meteorological and Hydrological Institute, Norrköping,
27 Sweden

28

29 **Key Points**

30 • There is good agreement between radiation budget variations observed by CERES and
31 simulated by seven state-of-the-art climate models

32 • The relationship between global mean net TOA radiation and surface temperature is
33 sensitive to changes in regions dominated by low clouds

34 • Most models underestimate shortwave flux changes in response to SST changes over
35 the east Pacific, suggesting too weak a “pattern effect”

36

37

* Corresponding Author: Norman G. Loeb, norman.g.loeb@nasa.gov; NASA Langley Research Center, Hampton, VA 21 Langley Boulevard, Hampton, VA 23681

38

Abstract

39 We compare top-of-atmosphere (TOA) radiative fluxes observed by the Clouds and the
40 Earth's Radiant Energy System (CERES) and simulated by seven general circulation
41 models forced with observed sea-surface temperature (SST) and sea-ice boundary
42 conditions. In response to increased SSTs along the equator and over the eastern Pacific
43 (EP) following the so-called global warming "hiatus" of the early 21st century, simulated
44 TOA flux changes are remarkably similar to CERES. Both show outgoing shortwave and
45 longwave TOA flux changes that largely cancel over the west and central tropical Pacific,
46 and large reductions in shortwave flux for EP low-cloud regions. A model's ability to
47 represent changes in the relationship between global mean net TOA flux and surface
48 temperature depends upon how well it represents shortwave flux changes in low-cloud
49 regions, with most showing too little sensitivity to EP SST changes, suggesting a "pattern
50 effect" that may be too weak compared to observations.

51

Plain Language Summary

52 Earth's radiation budget describes the balance between radiation from the sun intercepted
53 by Earth and radiation returned back to space through reflection of solar radiation and
54 emission of terrestrial thermal infrared radiation. This balance is a fundamental property
55 of Earth's climate system as it describes how Earth gains and sheds heat. Here we use
56 observations from the Clouds and the Earth's Radiant Energy System (CERES) to
57 evaluate how seven state-of-the-art climate models represent changes in Earth's radiation
58 budget during and following the so-called global warming "hiatus" of the early 21st
59 century. The models were provided observed sea-surface temperature and sea-ice
60 boundary conditions as well as natural and anthropogenic forcings. We find remarkable

61 agreement between observed and simulated differences in reflected solar and emitted
62 thermal infrared radiation between the post-hiatus and hiatus periods. Furthermore, a
63 model's ability to correctly relate Earth's radiation budget and surface temperature is
64 found to depend upon how well it represents reflected solar radiation changes in regions
65 dominated by low clouds, particularly those over the eastern Pacific ocean.

66

67

68 **1. Introduction**

69 A key measure of radiative feedback in the climate system, and therefore climate
70 sensitivity, is the relationship between net top-of-the-atmosphere (TOA) radiation and
71 global mean surface air temperature change. From climate model simulations in which
72 CO₂ is quadrupled instantaneously, the climate feedback parameter can be determined
73 from the slope of a linear regression fit between net flux and surface temperature change,
74 with the intercept yielding the imposed forcing (Gregory et al., 2004). This linear
75 framework assumes that the climate feedback parameter is constant in time, so that
76 variations in net flux and surface temperature are related by a constant of proportionality.
77 However, numerous modeling studies have shown that for transient warming, global
78 radiative feedback is time-varying (Murphy 1995; Senior and Mitchell 2000; Winton et
79 al. 2010; Armour et al. 2013; Andrews et al. 2015; Paynter et al. 2015; Gregory &
80 Andrews, 2016; Zhou et al., 2016; Armour, 2017; Proistosescu & Huybers, 2017; Marvel
81 et al., 2018; Silvers et al., 2018). This is primarily due to temporal changes in surface
82 warming patterns, which induce changes in global radiation that differ from those
83 associated with global warming (Armour et al., 2013; Rose et al., 2014; Andrews et al.,
84 2015; Zhou et al., 2016, 2017; Ceppi & Gregory, 2017; Haugstad et al., 2017; Andrews
85 & Webb, 2018; Silvers et al., 2018; Andrews et al. 2018; Dong et al. 2019). These
86 “pattern effects” (Stevens et al., 2016) can be a result of both internal variability and
87 climate forcing (Mauritsen, 2016).

88 The “pattern effect” is the reason why general circulation models (GCMs) driven
89 with historical patterns of sea-surface temperature (SST) and sea-ice concentrations (SIC)
90 yield climate feedback parameters that are more stabilizing—implying a lower climate

91 sensitivity—compared to simulations that are forced with projected long-term increases
92 in greenhouse gas concentrations (Zhou et al., 2016; Andrews et al., 2018; Marvel et al.,
93 2018). While global mean surface temperatures have been continuing to increase in
94 recent decades, there has been relatively less warming (or even cooling) over the eastern
95 tropical Pacific (e.g., McGregor et al., 2014) and Southern Oceans (e.g., Armour et al.,
96 2016). These regional patterns have been shown to produce greater low-level cloud cover
97 and reflection to space, explaining why there was a more stabilizing climate feedback
98 parameter observed during this time period compared to that of future warming (Zhou et
99 al., 2016, 2017; Andrews et al., 2018; Dong et al. 2019). Zhou et al. (2016) further argue
100 that SST pattern-induced low-cloud cover anomalies may have also contributed to
101 reduced warming between 1998 and 2013, a period that has come to be known as the
102 global warming “hiatus” (e.g., McGregor et al., 2014). More recently, Fueglistaler (2019)
103 demonstrated the influence of SST pattern changes on observed tropical mean SW cloud
104 radiative effect using data from the Clouds and the Earth’s Radiant Energy System
105 (CERES).

106 In this study, we use CERES observations to evaluate how state-of-the-art climate
107 models represent changes in Earth’s radiation budget following a large change in SST
108 patterns. The CERES data reveal a 0.83 Wm^{-2} reduction in global mean reflected
109 shortwave (SW) flux during the three years following the hiatus, resulting in an increase
110 in net energy into the climate system (Loeb et al., 2018a). Furthermore, decreases in low-
111 cloud cover are found to be the primary driver of the decrease in SW flux. The low-cloud
112 cover decreases are associated with increases in SST reaching 2°C on average in some

113 locations over the eastern Pacific Ocean following a change in the sign of the Pacific
114 Decadal Oscillation from negative to positive phase.

115 In light of these dramatic changes, we ask the question: can climate models
116 reproduce the changes observed by CERES if they are provided observed SSTs and SIC?
117 Such a comparison serves as a “reality check” on the models used to study the pattern
118 effect, low-cloud feedbacks and changes in total climate feedback during the historical
119 period. We caution that there is no attempt here to provide an “emergent constraint” on
120 future climate (Klein and Hall, 2015) that can be used to constrain long-term climate
121 feedback and climate sensitivity. Rather, the goal is to determine whether or not current
122 atmospheric models are capable of reproducing the TOA radiative response to a large-
123 scale and well-observed event that arguably involves processes relevant to the
124 representation of both current and future climate.

125 **2. Data and Methods**

126 **2.1 Observations**

127 We use observational data from the CERES EBAF Ed4.1 product (Loeb et al.,
128 2018b, 2019) for March 2000–December 2017. EBAF provides monthly mean TOA and
129 surface SW and longwave (LW) radiative fluxes on a $1^\circ \times 1^\circ$ grid. Here, only the TOA
130 fluxes are considered. TOA radiative fluxes in EBAF are derived from CERES SW and
131 LW radiance measurements.

132 Also considered are atmospheric and surface data from the European Centre for
133 Medium-Range Weather Forecasts ERA5 reanalysis product (Hersbach et al., 2018). We
134 use near-surface air temperature (T_s), surface pressure, 700 hPa air temperature and SST.

135 The first three parameters are used to calculate the estimated inversion strength (EIS)
136 (Wood and Bretherton, 2006).

137 **2.2 CMIP6 AMIP Simulations**

138 TOA radiative fluxes, T_s and EIS from seven models participating in the Coupled
139 Model Intercomparison Project Phase 6 (CMIP6; Eyring et al., 2016) are considered
140 (Table 1). The simulations are forced with monthly time-varying observationally derived
141 fields of SST and SIC using the Atmospheric Model Intercomparison Project (AMIP)
142 boundary conditions (Gates et al., 1999; Hurrell et al., 2008; Taylor et al., 2000).
143 Between the start of the CERES record in 2000 and the official end-date of CMIP6 AMIP
144 in 2014, all simulations have time-varying natural and anthropogenic forcings. We have
145 run AMIP simulations three more years, through the end of 2017. In those simulations,
146 radiative forcings are held fixed at 2014 levels between 2015-2017 for all models except
147 EC-Earth3-Veg, which used the Shared Socioeconomic Pathways (SSP2-4.5) radiative
148 forcings (Riahi et al., 2016). Monthly time-varying observed fields of SST and SIC from
149 either merged Reynolds/HADISST (Hurrell et al., 2008) or HadISST1 (Rayner et al.,
150 2003) are used (Table 1). All AMIP simulation output are spatially interpolated onto a
151 $1^\circ \times 1^\circ$ grid.

152 Since AMIP simulations use observed SSTs and SIC boundary conditions, the
153 model atmosphere responds to SSTs but there is no equivalent ocean surface response to
154 atmospheric changes. This is in contrast to observations, which include two-way
155 atmosphere-ocean interactions. A reasonable question to ask, therefore, is whether it is
156 reasonable to evaluate models by comparing AMIP simulations and observations. This
157 has been addressed in several studies with different models (Andrews et al., 2015; He and

158 Soden, 2016; Haugstad et al., 2017; Mauritsen and Stevens, 2015). The studies find that
 159 time-varying net feedback parameters simulated by atmosphere-ocean GCMs (AOGCMs)
 160 and AMIP-style simulations for the same models forced using the AOGCM SST and SIC
 161 boundary conditions are consistent, suggesting that AMIP-style simulations and
 162 observations should also show consistent results.

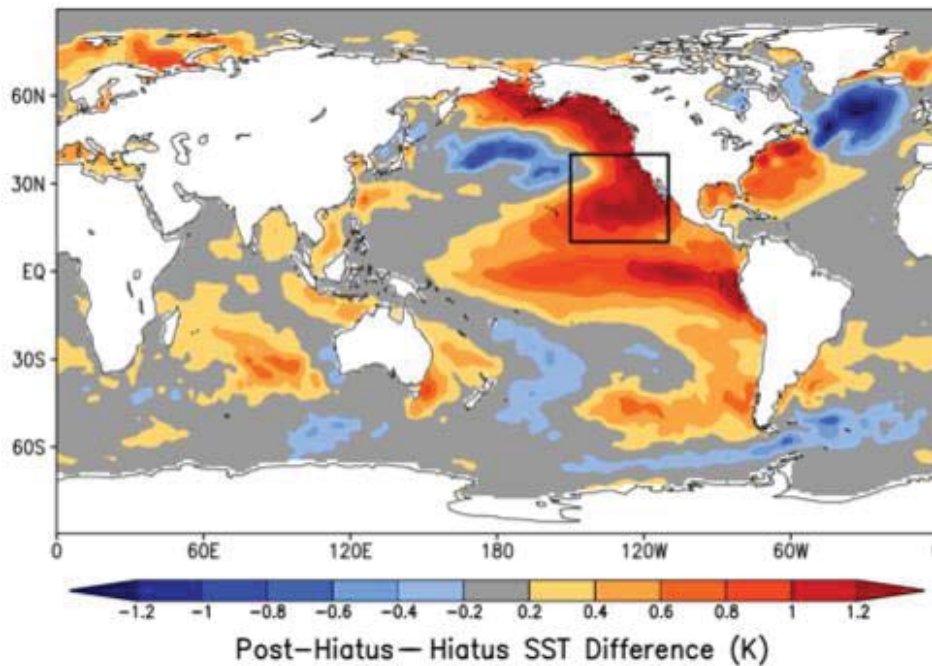
163 Table 1 List of CMIP6 models considered in this study.

Model (Short Name)	Model (Long Name)	Country	Resolution (°) (lonxlat)	SST/SIC Dataset	Reference
CESM2	CESM2 AMIP	USA	1.25x0.94	Merged Reynolds/HADISST	Gettelman et al. (2019)
CanESM5	CanESM5 AMIP	Canada	2.8x2.8	Merged Reynolds/HADISST	Swart et al. (2019)
EC-Earth3-Veg	EC-Earth3-Veg AMIP	Europe/EC	0.7x0.7	Merged Reynolds/HADISST	Davini et al. (2017)
ECHAM6.3	echam6.3.05-LR AMIP	Germany	1.875x1.86	HadISST1	Mauritsen et al. (2019)
GFDL-AM4	GFDL-AM4 AMIP	USA	1.25x1.0	HadISST1	Zhao et al. (2018)
HadGEM3	HadGEM3-GC31-LL AMIP	UK	1.875x1.25	HadISST1	Williams et al. (2018)
IPSL-CM6A	IPSL-CM6A-LR AMIP	France	2.5x1.27	Merged Reynolds/HADISST	Hourdin et al. (2013)

164 2.3 Methods

165 Deseasonalized monthly anomalies are determined by differencing the average in
 166 a given month from the average of all years of the same month. We consider TOA flux
 167 differences between means for the post-hiatus and hiatus periods, where the hiatus period
 168 is defined as July 2000–June 2014 and the post-hiatus period is July 2014–June 2017.

169 The corresponding SST difference pattern (Figure 1) shows marked SST increases during
170 the post-hiatus period along the entire coast of North America, central Pacific Ocean, and
171 to a lesser extent, along the coast of South America. In addition to examining global
172 results, we also investigate how the models capture flux changes in a domain dominated
173 primarily by low clouds over the eastern Pacific (EP) (see box in Figure 1).



174 **Figure 1.** Post-hiatus—hiatus difference in sea-surface temperature. The black box shows
175 the EP domain defined by 10°N-40°N and 150°W-110°W.
176

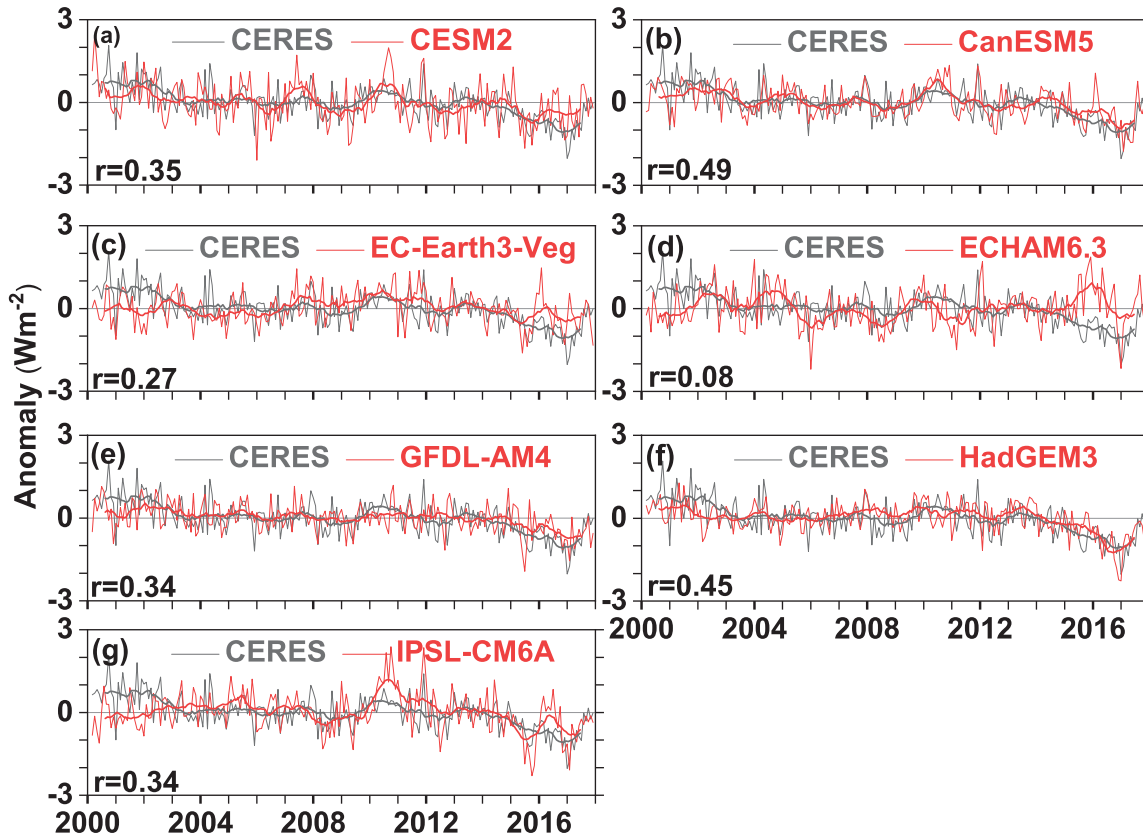
177 3. Results

178 3.1 Global TOA Flux Anomalies

179 A comparison between SW flux anomalies from CERES and the seven CMIP6
180 models is provided in Figures 2a-g, with positive numbers indicating anomalous upward
181 radiation at the TOA. The corresponding comparisons for LW upward and net downward
182 fluxes are shown in Figures S1 and S2. The CERES observations show appreciable
183 positive SW and negative LW anomalies at the beginning of the CERES record,
184 following a period of prolonged La Niña conditions that started in mid-1998 and ended in

185 mid-2001. Anomalies remain fairly weak between 2002 and 2013. Starting in 2014, a
186 marked trend toward negative SW anomalies occurs that reaches a minimum value in
187 January 2017, one year after the peak of the 2015/2016 El Niño event (one of the largest
188 on record). SW anomalies return to near-normal levels at the end of 2017.

189 The CanESM5 and HadGEM3 models track the observed SW anomalies
190 remarkably well during the entire period. All models except ECHAM6.3 capture the large
191 negative SW flux anomalies during the post-hiatus period, but many fail to reproduce the
192 large positive anomalies at the beginning of the CERES record. While the overall mean
193 correlation coefficient between model and observed monthly SW anomalies is only
194 0.33 ± 0.098 , the standard deviation in CMIP6 SW monthly anomalies is consistent with
195 CERES (Table S1). For LW and net, most of the models closely track the CERES 12-
196 month running average, but they are less successful at capturing monthly variations.
197 When annual anomalies are considered, model-observed correlation coefficients increase
198 by a factor of 2 (Table S1). This is likely because more of the variability at annual time-
199 scales is driven by interannual variability in the SST boundary conditions, whereas
200 significant sub-annual variability is due to atmospheric stochastic variability, which is
201 poorly correlated between models and observations (Proistosescu et al., 2018).



202

203 **Figure 2.** Deseasonalized anomalies in global mean TOA SW upward flux for CERES
 204 and each of the seven CMIP6 models considered in Table 1. Thin lines correspond to
 205 monthly anomalies; thick lines are 12-month running averages. Correlation
 206 coefficients (r) between model and observed monthly anomalies are also shown.

207

208 **3.2 Post-Hiatus—Hiatus Differences**

209

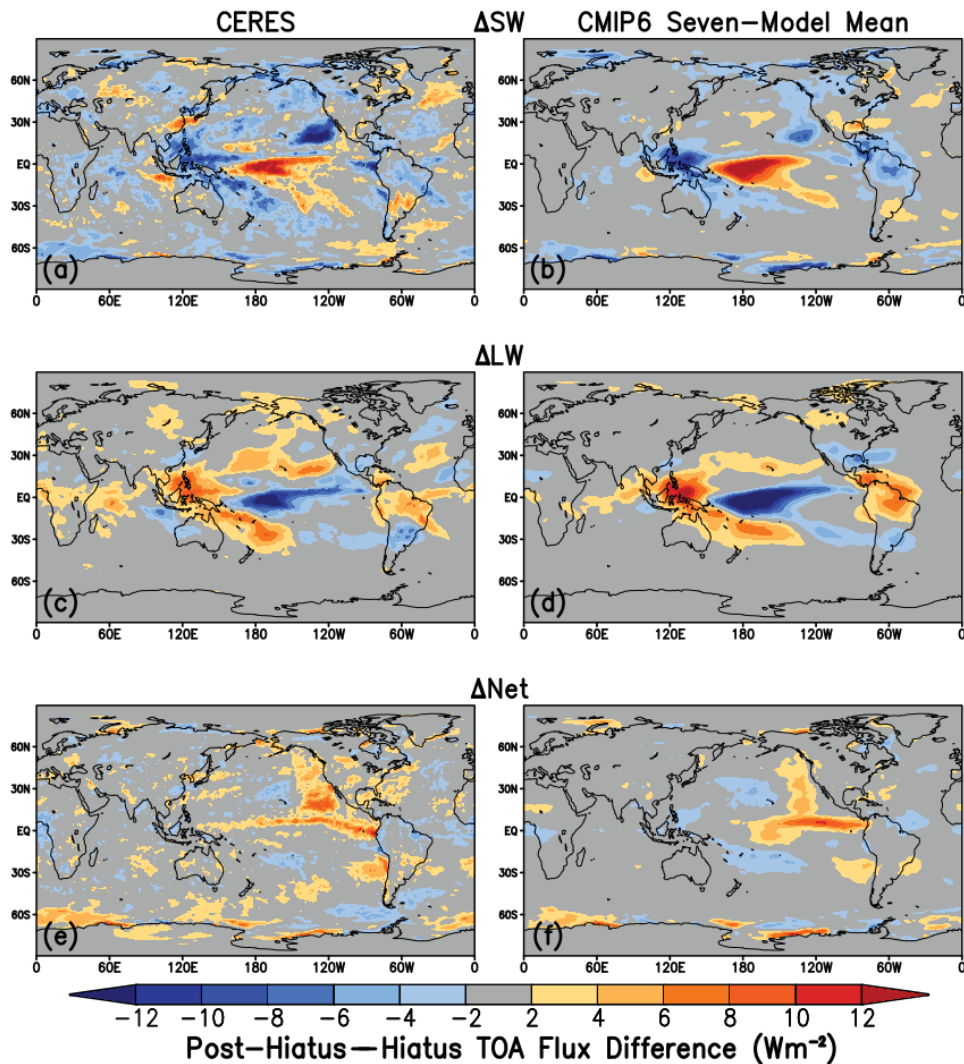
We find encouraging similarities between regional patterns of post-hiatus—hiatus
 210 flux difference for CERES and the mean of the seven CMIP6 models (Figure 3a-f). The
 211 CERES observations show a marked SW decrease during the post-hiatus period off the
 212 west coast of North America (Figure 3a), a region characterized by persistent marine
 213 stratocumulus. Surface warming in the East Pacific reduces the vertical stratification,
 214 which reduces low-cloud cover (Klein and Hartmann 1993) and reflected solar radiation.
 215 Large decreases in low-cloud cover in this region are thought to have played a significant
 216 role in causing record-breaking warm SST anomalies after 2014 (Johnson and Birnbaum,

217 2016; Myers et al., 2018). In the tropics, CERES shows positive SW and negative LW
218 differences in the central Pacific, and differences of the opposite sign in the western
219 Pacific (Figures 3a and 3c). These patterns are consistent with an eastward shift in the
220 location of tropical convection during the 2015/2016 El Niño event. The marked SW and
221 LW tropical differences largely cancel, however, and are thus less prominent in the
222 regional distribution of net flux differences (Figure 3e). Large positive net flux
223 differences appear off the west coast of North America since cancellation between SW
224 and LW is weaker there.

225 The flux difference pattern for the mean of the seven CMIP6 models shows a
226 striking resemblance to CERES (Figures 3b, 3d and 3f). Like CERES, the CMIP6 mean
227 SW flux decreases in the region of large SST increase off the west coast of North
228 America (Figure 3b). However, the magnitude of the decrease is weaker than CERES.
229 Results for the individual models show that CanESM5 and HadGEM3 produce SW flux
230 decreases that are larger than the 7-model mean and occur in the same location as CERES
231 (Figure S3). Large decreases also occur for IPSL-CM6A and CESM2, but the locations
232 differ from CERES. These results are qualitatively consistent with other satellite studies
233 that found a negative correlation between low-cloud cover and SST from passive (Myers
234 and Norris, 2015; Qu et al., 2015; McCoy et al., 2017; Yuan et al., 2018) and active
235 sensors (Myers and Norris, 2015; Cesana et al., 2019).

236 In the tropics, the locations of negative SW and positive LW anomalies in the
237 South Pacific Convergence Zone (SPCZ) and Maritime Continent, and positive SW and
238 negative LW anomalies in the central Pacific coincide with CERES (Figures 3a-d).
239 However, the magnitudes of the CMIP6 model anomalies are larger than CERES both for

240 the seven-model mean (Figures 3a-b) and most of the models individually (Figures S3-
 241 S4). The CMIP6 model mean reproduces the large positive net downward flux anomalies
 242 off the west coast of North America and along the equator seen in CERES (Figure 3e-f,
 243 Figure S5).



244
 245 **Figure 3.** Post-hiatus—hiatus difference in (a, b) SW upward, (c, d) LW upward and (e,
 246 f) net downward TOA flux for CERES (left column) and average of seven CMIP6
 247 model simulations (right column).

248 When averaged globally, all CMIP6 models except ECHAM6.3 show negative
 249 SW and positive LW upward flux differences between the post-hiatus and hiatus periods,
 250 consistent with CERES (Figure S6). The ECHAM6.3 model underestimates the

251 magnitude of negative SW differences associated with decreases in low clouds off the
252 west coast of North America and convection over the western tropical Pacific yet shows
253 strong positive SW (and negative LW) differences in the central tropical Pacific and over
254 North America, resembling a slight geographical shift of tropical convection in the zonal
255 direction (Figures S3e, S4e). Excluding ECHAM6.3, the root-mean-square difference of
256 the other six CMIP6 models relative to CERES is 0.3 Wm^{-2} and 0.15 Wm^{-2} for SW and
257 LW, respectively. The model most consistent with CERES is HadGEM3, which in
258 addition to producing very similar global mean post-hiatus—hiatus differences,
259 reproduces observed regional patterns rather well.

260 In the EP domain, the post-hiatus—hiatus difference in reflected SW flux is
261 almost entirely associated with changes in T_s , based upon a multivariate regression
262 analysis of SW against T_s and EIS (see Supporting Information). All of the models have a
263 T_s contribution to the SW flux difference that is too weak compared to the observations
264 (Figure S7). We also find little correlation between how well a model represents the SW
265 flux post-hiatus—hiatus difference in the EP domain and the corresponding
266 climatological mean value (Figure S11). The CESM2 model shows the greatest
267 climatological mean bias (-10 Wm^{-2}) yet its bias in the post-hiatus—hiatus difference is
268 only 1 Wm^{-2} . In contrast, EC-Earth3-Veg shows a climatological mean bias of 2 Wm^{-2}
269 and a post-hiatus—hiatus difference of 4 Wm^{-2} . Notably, all of the models but two
270 (ECHAM6.3 and IPSL-CM6A) have negative biases in the climatological mean SW flux.
271 This is consistent with earlier studies that have shown models having a tendency to
272 underestimate low-cloud cover in the subtropical stratocumulus regions off the west
273 coasts of North and South America and Africa (Zhao et al., 2018). These results imply

274 that good agreement between observed and model climatology does not necessarily imply
275 good agreement in climate variability.

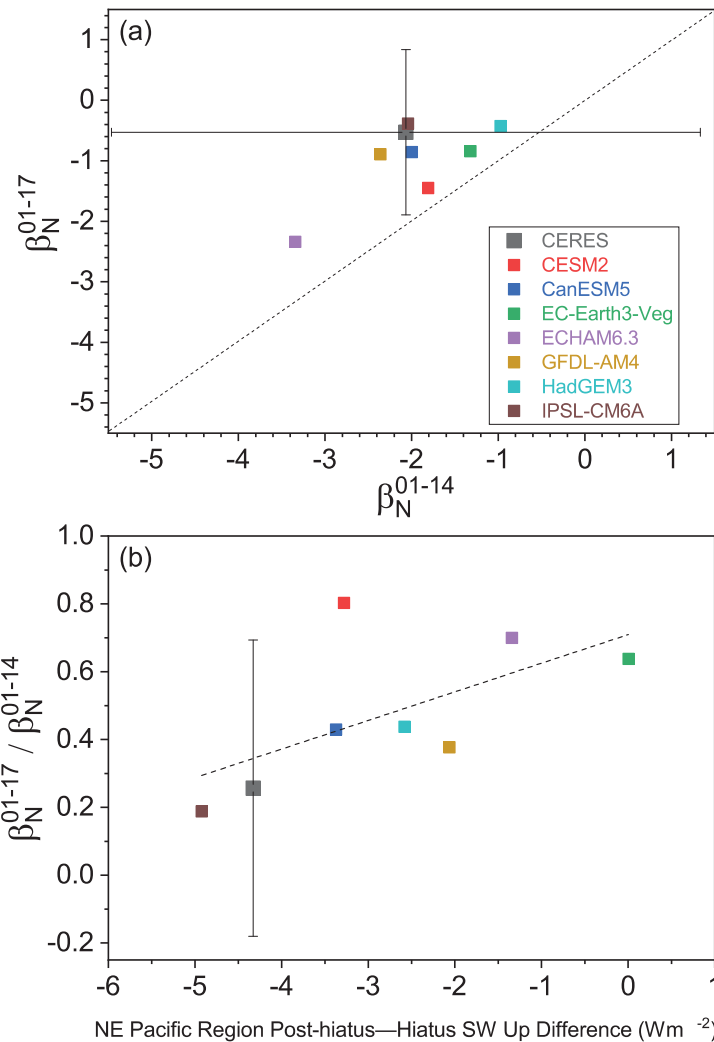
276 **3.3 Pattern Effect**

277 To examine the influence of the SST pattern change during the CERES period
278 (Figure 1) on the relationship between net flux and surface temperature, we use an
279 approach similar to Andrews et al (2018), who demonstrated the influence of the pattern
280 effect on the net climate feedback parameter (λ_N) for the historical record (1871-2010)
281 and long-term CO₂ forcing. We refer to a radiative restoring coefficient (Lutsko and
282 Takahashi, 2018) for the CERES period (β_N) instead of λ_N in order to emphasize that β_N
283 is primarily a response to internal variability in the climate system whereas λ_N is
284 primarily a response to external radiative forcing. We define β_N as $\beta_N = (\delta N - \delta F) /$
285 δT_s , where δN is net flux anomaly, δF is the effective radiative forcing anomaly and δT_s
286 is the surface temperature anomaly. Here, δ are annual anomalies over the CERES
287 period. F is obtained from the Intergovernmental Panel on Climate Change (IPCC) Fifth
288 Assessment Report (AR5) forcing time series updated and extended following Dessler
289 and Forster (2018). We determine β_N for 2001-2017 and 2001-2014 from CERES and
290 each of the seven CMIP6 models by calculating the slope of $\delta N - \delta F$ against δT_s using a
291 standard ordinary least squares fit. To calculate δF , the same time-varying F is assumed
292 for CERES and each CMIP6 model through 2014. For 2015-2017, F is held fixed at the
293 2014 value for the CMIP6 models but is time-varying for CERES. The uncertainty in the
294 regression slope is represented by its 95% confidence interval.

295 For CERES, β_N becomes dramatically less stabilizing when the three post-hiatus
296 years are included (Figure 4a), changing from $-2.1 \text{ Wm}^{-2} \text{ K}^{-1}$ (-5.5 to $1.3 \text{ Wm}^{-2} \text{ K}^{-1}$) for

297 2001-2014 to $-0.53 \text{ Wm}^{-2} \text{ K}^{-1}$ (-1.9 to $0.83 \text{ Wm}^{-2} \text{ K}^{-1}$) for 2001-2017. The change in β_N
298 is mainly due to a strong positive SW feedback (Figure S12) associated with the large
299 decrease in global mean reflected SW flux during the post-hiatus period. We note that the
300 95% confidence intervals in β_N for these short periods are large owing to the short record
301 of CERES. With the exception of ECHAM6.3, all of the model β_N values for 2001-2017
302 fall within the 95% confidence interval of the observations. Excluding ECHAM6.3, the
303 mean of the other six models have a less stabilizing β_N compared to CERES for 2001-
304 2014 by $0.3 \text{ Wm}^{-2} \text{ K}^{-1}$ and a more stabilizing β_N by approximately the same magnitude
305 for 2001-2017.

306 We quantify the pattern effect during the CERES period as the ratio of β_N for
307 2001-2017 to that for 2001-2014. This ratio is plotted against the post-hiatus—hiatus
308 difference in SW upward flux for the EP domain in Figure 4b. The IPSL-CM6A model
309 shows remarkable agreement with CERES, whereas the other models have both a β_N
310 ratio that is too large, indicating too weak a pattern effect, corresponding to too weak a
311 SW response in the EP domain. The positive correlation in Figure 4b suggests that at
312 least for these periods, a model's ability to represent changes in the relationship between
313 global mean net flux and surface temperature (and therefore the pattern effect) depends
314 critically upon how well it represents SW flux changes in low-cloud regions.



315

316 **Figure 4.** (a) Global net climate feedback parameter for 2001-2017 against that for 2001-
 317 2014. (b) Ratio of 2001-2017 and 2001-2014 global net climate feedback parameters
 318 against NE Pacific region post-hiatus—hiatus SW up difference. Dashed lines
 319 correspond to one-to-one line in (a) and linear regression fit to all points in (b).

320 **4. Conclusions**

321

322

The general agreement between TOA radiation changes simulated by the seven
 323 CMIP6 AGCMs considered in this study and CERES is encouraging as it suggests that
 324 the models' atmospheric response to large-scale SST pattern changes resulting from a
 325 combination of internal and forced variations is realistic. We find that a model's ability to

326 represent changes in the relationship between global mean flux and surface temperature
327 depends critically upon how well it represents SW flux changes in regions dominated by
328 low clouds, such as the EP domain considered here. Part of the reason is because there is
329 less cancellation between SW and LW flux changes in these regions compared to the
330 west and central Pacific, where marked SW and LW differences are quite similar in
331 magnitude but opposite in sign. Over longer timescales, coupled climate model
332 simulations also suggest an important role for low clouds in determining the future
333 climate state. However, model biases could play a critical role (McGregor et al. 2018) in
334 explaining why coupled models are not able to simulate the observed SST pattern during
335 the hiatus (McGregor et al. 2014, Coats and Karnauskas, 2017). We thus caution that
336 consistency between AGCM simulations and observations at interannual timescales is not
337 a guarantee of success in projecting future climate, as other processes operating at longer
338 timescales likely also matter.

339 **Acknowledgements**

340 N.G.L. and H.W. were supported by the NASA CERES project. R.P.A. was supported by
341 the UK National Environment Research Council (NERC) SMURPHS project
342 (NE/N006054/1). TA was supported by the Met Office Hadley Centre Climate
343 Programme funded by BEIS and Defra. A.G. was supported by The National Center for
344 Atmospheric Research, which is sponsored by the U.S. National Science Foundation.
345 T.M. acknowledges funding from the European Research Council grant #770765 and
346 European Union Horizon 2020 project #820829 EBAF Ed4.1 data was downloaded
347 online from: <https://ceres.larc.nasa.gov/products-info.php?product=EBAF>. ERA5 data
348 from the European Centre for Medium-range Weather Forecast (ECMWF) was
349 downloaded online from: [https://www.ecmwf.int/en/forecasts/datasets/reanalysis-](https://www.ecmwf.int/en/forecasts/datasets/reanalysis-datasets/era5)
350 [datasets/era5](https://www.ecmwf.int/en/forecasts/datasets/reanalysis-datasets/era5). The EC-Earth3-Veg simulations were performed on resources provided by
351 the Swedish National Infrastructure for Computing (SNIC).

352 **References**

353

354 Andrews, T., Gregory, J. M., Paynter, D., Silvers, L. G., Zhou, C., Mauritsen, T., et al.
355 (2018). Accounting for changing temperature patterns increases historical estimates
356 of climate sensitivity. *Geophysical Research Letters*, 45, 8490–8499.
357 <https://doi.org/10.1029/2018GL078887>.

358

359 Andrews, T., Gregory, J. M., & Webb, M. J. (2015). The dependence of radiative forcing
360 and feedback on evolving patterns of surface temperature change in climate models.
361 *Journal of Climate*, 28(4), 1630–1648. <https://doi.org/10.1175/jcli-d-14-00545.1>.

362

363 Andrews, T., & Webb, M. J. (2018). The dependence of global cloud and lapse rate
364 feedbacks on the spatial structure of tropical Pacific warming. *Journal of Climate*,
365 31(2), 641–654. <https://doi.org/10.1175/JCLI-D-17-0087>.

366

367 Armour, K. C., Bitz, C. M., & Roe, G. H. (2013). Time-varying climate sensitivity from
368 regional feedbacks. *Journal of Climate*, 26(13), 4518–4534.
369 <https://doi.org/10.1175/JCLI-D-12-00544.1>.

370

371 Armour, K. C., J. Marshall, J. R. Scott, A. Donohoe, and E. R. Newsom (2016), Southern
372 Ocean warming delayed by circumpolar upwelling and equatorward transport, *Nature*
373 *Geoscience*, 9, 549–554, doi: [10.1038/ngeo2731](https://doi.org/10.1038/ngeo2731)

374

375 Armour, K. C. (2017). Energy budget constraints on climate sensitivity in light of
376 inconstant climate feedbacks. *Nature Climate Change*, 7(5), 331–335.
377 <https://doi.org/10.1038/nclimate3278>.

378

379 Ceppi, P., & Gregory, J. M. (2017). Relationship of tropospheric stability to climate
380 sensitivity and Earth's observed radiation budget. *Proceedings of the National*
381 *Academy of Sciences of the United States of America*, 114(50), 13,126–13,131.
382 <https://doi.org/10.1073/pnas.1714308114>

383

384 Cesana, G., and D. E. Waliser (2016), Characterizing and understanding systematic
385 biases in the vertical structure of clouds in CMIP5/CFMIP2 models, *Geophys.*
386 *Res. Lett.*, 43, 10,538–10,546, doi:10.1002/2016GL070515.

387

388 Cesana, G., A. D. Del Genio, A. S. Ackerman, M. Kelley, G. Elsaesser, A. M. Fridlind, Y.
389 Cheng, and M.-S. Yao (2019), Evaluating models' response of tropical low clouds
390 to SST forcings using CALIPSO observations. *Atmos. Chem. Phys.*, 19, 2813–2832.
391 <https://doi.org/10.5194/acp-19-2813-2019>.

392

393 Coats, S., & Karnauskas, K. B. (2017). Are simulated and observed twentieth century
394 tropical Pacific sea surface temperature trends significant relative to internal
395 variability? *Geophysical Research Letters*, 44, 9928–9937.
396 <https://doi.org/10.1002/2017GL074622>

397

398
399 Dessler, A. E., and Forster, P. M. (2018). An estimate of equilibrium climate
400 sensitivity from interannual variability. *J. Geophys. Res. Atmos.*
401 doi:10.1029/2018JD028481.
402
403 Davini, P., and Coauthors, 2017: Climate SPHINX: evaluating the impact of resolution
404 and stochastic physics parameterisations in the EC-Earth global climate model.
405 *Geosci Model Dev.* 10(3):1383.
406
407 Dong, Y., Proistosescu, C., Armour, K. C. & Battisti, D. S. (2019): Attributing historical
408 and future evolution of radiative feedbacks to regional warming patterns using a
409 green's function approach: The preeminence of the Western Pacific. *Journal of*
410 *Climate*, 32, 5471-5491. doi: 10.1175/JCLI-D-18-0843.1.
411
412 Eyring, V., Bony, S., Meehl, G. A., Senior, C. A., Stevens, B., Stouffer, R. J., and Taylor, K.
413 E. (2016). Overview of the Coupled Model Intercomparison Project Phase 6
414 (CMIP6) experimental design and organization, *Geosci. Model Dev.*, 9, 1937-
415 1958, <https://doi.org/10.5194/gmd-9-1937-2016>
416
417 Fueglistaler, S. (2019). Observational evidence for two modes of coupling between sea
418 surface temperatures, tropospheric temperature profile, and shortwave cloud radiative
419 effect in the tropics. *Geophysical Research Letters*, 46.
420 <https://doi.org/10.1029/2019GL083990>
421
422 Gates, W. L., Boyle, J. S., Covey, C., Dease, C. G., Doutriaux, C. M., Drach, R. S., et al.
423 (1999). An overview of the results of the Atmospheric Model Intercomparison Project
424 (AMIP I). *Bulletin of the American Meteorological Society*, 80(1), 29–55.
425 [https://doi.org/10.1175/1520-0477\(1999\)080<0029:AOOTRO>2.0.CO;2](https://doi.org/10.1175/1520-0477(1999)080<0029:AOOTRO>2.0.CO;2)
426
427 Gettelman, A., Hannay, C., Bacmeister, J. T., Neale, R. B., Pendergrass, A. G.,
428 Danabasoglu, G., et al. (2019). High Climate Sensitivity in the Community Earth
429 System Model Version 2 (CESM2). *Geophys. Res. Lett.* 46, 8329–8337.
430 doi:10.1029/2019gl083978
431
432 Gregory, J. M., & Andrews, T. (2016). Variation in climate sensitivity and feedback
433 parameters during the historical period. *Geophysical Research Letters*, 43, 3911–
434 3920. <https://doi.org/10.1002/2016GL068406>.
435
436 Haugstad, A. D., Armour, K. C., Battisti, D. S., & Rose, B. E. J. (2017). Relative roles of
437 surface temperature and climate forcing patterns in the inconstancy of radiative
438 feedbacks. *Geophysical Research Letters*, 44, 7455–7463.
439 <https://doi.org/10.1002/2017GL074372>
440
441 He, J., & Soden, B. J. (2016). Does the lack of coupling in SST-forced atmosphere-only
442 models limit their usefulness for climate change studies? *Journal of Climate*, 29,
443 4317-4325. <http://dx.doi.org/10.1175/JCLI-D-14-00597.s1>

444
445 Hersbach, H., et al., 2018: Operational global reanalysis: progress, future directions and
446 synergies with NWP. ERA Report Series. European Centre for Medium Range
447 Weather Forecasts. Reading, UK. [Available from:
448 <https://www.ecmwf.int/file/276463/download?token=q6uGbnPD>]
449
450 Hourdin H, et al. (2013): LMDZ5B: The atmospheric component of the IPSL climate
451 model with revisited parameterizations for clouds and convection. *Climate Dynamics*,
452 40, 2193-2222. <https://doi.org/10.1007/s00382-012-1343-y>.
453
454 Hurrell, J., Hack, J., Shea, D., Caron, J., & Rosinski, J. (2008). A new sea surface
455 temperature and sea ice boundary dataset for the community atmosphere model.
456 *Journal of Climate*, 21(19), 5145–5153. <https://doi.org/10.1175/2008JCLI2292.1>.
457
458 Johnson, G. C., and A. N. Birnbaum (2017), As El Niño builds, Pacific Warm Pool
459 expands, ocean gains more heat, *Geophys. Res. Lett.*, 44, 438–445,
460 doi:10.1002/2016GL071767.
461
462 Klein, S. A., Hall, A. (2015). Emergent constraints for cloud feedbacks. *Curr. Clim.*
463 *Change Rep.*, 1:276–287. <https://doi.org/10.1007/s40641-015-0027-1>
464
465 Klein, S. A., & Hartmann, D. L. (1993). The seasonal cycle of low stratiform clouds.
466 *Journal of Climate*, 6, 1587-1606.
467
468 Loeb, N. G., Thorsen, T. J., Norris, J. R., Wang, H., & Su, W. (2018a). Changes in
469 earth’s energy budget during and after the “Pause” in Global Warming: An
470 observational perspective. *MDPI Climate*, 6, 62; doi:10.3390/cli6030062.
471
472 Loeb, N. G., D. R. Doelling, H. Wang, W. Su, C. Nguyen, J. G. Corbett, L. Liang, C.
473 Mitrescu, F. G. Rose, and S. Kato, 2018b: Clouds and the Earth’s Radiant Energy
474 System (CERES) Energy Balanced and Filled (EBAF) Top-of-Atmosphere (TOA)
475 Edition 4.0 data product, *J. Climate*, 31, 895-918. doi:10.1175/JCLI-D-17-0208.1.
476
477 Loeb, N.G., F.G. Rose, S. Kato, D.A. Rutan, W. Su, H. Wang, D.R. Doelling, W.L.
478 Smith, Jr., and A. Gettelman, 2019: Towards a consistent definition between satellite
479 and model clear-sky radiative fluxes. *J. Climate*, 33, 61-75. doi: 10.1175/JCLI-D-19-
480 0381.1.
481
482 Lutsko, N. J., & Takahashi, K. (2018). What can the internal variability of CMIP5
483 models tell us about their climate sensitivity? *Journal of Climate*, 31, 5051-5069.
484 doi:10.1175/JCLI-D-17-0736.1
485
486 Marvel, K., Pincus, R., Schmidt, G. A., & Miller, R. L. (2018). Internal variability and
487 disequilibrium confound estimates of climate sensitivity from observations.
488 *Geophysical Research Letters*, 45, 1595–1601.
489 <https://doi.org/10.1002/2017GL076468>.

490
491 Mauritsen, T., (2016). Clouds cooled the Earth. *Nature Geoscience*, 9, 865-867.
492
493 Mauritsen, T., Bader, J., Becker, T., Behrens, J., Bittner, M., Brokopf, R., et al. (2019).
494 Developments in the MPI-M Earth System Model version 1.2 (MPI-ESM1.2) and its
495 response to increasing CO₂. *Journal of Advances in Modeling Earth Systems*, 11,
496 998–1038. <https://doi.org/10.1029/2018MS001400>.
497
498 Mauritsen, T., & Stevens, B. (2015). Missing iris effect as a possible cause of muted
499 hydrological change and high climate sensitivity in models. *Nature Geoscience*, 8,
500 346-351. doi:10.1038/NGEO2414
501
502 McCoy, D. T., Eastman, R., Hartmann, D. L., and Wood, R.: The Change in Low Cloud
503 Cover in a Warmed Climate Inferred from AIRS, MODIS, and ERA-Interim, *J.*
504 *Climate*, 30, 3609–3620, <https://doi.org/10.1175/JCLI-D-15-0734.1>, 2017.
505
506 McGregor, S., A. Timmermann, M. F. Stuecker, M. H. England, M. Merrifield, F.-F. Jin,
507 and Y. Chikamoto (2014), Recent Walker circulation strengthening and Pacific
508 cooling amplified by Atlantic warming, *Nature Climate Change*, 4, 888–892,
509 doi:10.1038/nclimate2330.
510
511 McGregor, S., M. F. Stuecker, J. B. Kajtar, M. H. England, & M. Collins (2018): Model
512 Tropical Atlantic biases underpin diminished Pacific decadal variability, *Nature*
513 *Climate Change*, 8, 493–498, doi:10.1038/s41558-018-0163-4.
514
515 Murphy, J. M. (1995): Transient response of the Hadley Centre Coupled Ocean-
516 Atmosphere Model to increasing carbon dioxide. Part 1: Control climate and flux
517 adjustment. *Journal of Climate*, 8, 36-56. doi:10.1175/1520-
518 0442(1995)008<0036:TROTHC>2.0.CO;2
519
520 Myers, T. A., Mechoso, C. R., Cesana, G. V., DeFlorio, M. J., & Waliser, D. E. (2018).
521 Cloud feedback key to marine heatwave off Baja California. *Geophysical Research*
522 *Letters*, 45, 4345–4352. <https://doi.org/10.1029/2018GL078242>.
523
524 Myers, T. A., and J. R. Norris (2016), Reducing the uncertainty in subtropical cloud
525 feedback, *Geophys. Res. Lett.*, 43,2144–2148, doi:10.1002/2015GL067416.
526
527 Myers, T. A., and J. R. Norris (2015), On the relationships between subtropical clouds
528 and meteorology in observations and CMIP3 and CMIP5 models, *J. Clim.*, 28, 2945–
529 2967.
530
531 Paynter, D., and T. L. Frölicher (2015), Sensitivity of radiative forcing, ocean heat
532 uptake, and climate feedback to changes in anthropogenic greenhouse gases and
533 aerosols, *J. Geophys. Res. Atmos.*, 120, 9837–9854, doi:10.1002/2015JD023364.
534

535 Proistosescu, C., & Huybers, P. J. (2017). Slow climate mode reconciles historical and
536 model-based estimates of climate sensitivity. *Science Advances*, 3(7), e1602821.
537 <https://doi.org/10.1126/sciadv.1602821>.
538

539 Proistosescu, C., Donohoe, A., Armour, K. C., Roe, G. H., Stuecker, M. F., & Bitz, C. M.
540 (2018). Radiative feedbacks from stochastic variability in surface temperature and
541 radiative imbalance. *Geophysical Research Letters*, 45, 5082–5094.
542 <https://doi.org/10.1029/2018GL077678>
543

544 Qu, X., A. Hall, S. A. Klein, and A. M. DeAngelis (2015), Positive tropical marine low-
545 cloud cover feedback inferred from cloud controlling factors, *Geophys. Res. Lett.*, 42,
546 7767–7775, doi:10.1002/2015GL065627.
547

548 Rayner, N. A., Parker, D. E., Horton, E. B., Folland, C. K., Alexander, L. V., Rowell, D.
549 P., Kent, E. C., and Kaplan, A. (2003) Global analyses of sea surface temperature, sea
550 ice, and night marine air temperature since the late nineteenth century, *J. Geophys.*
551 *Res.*, 108(D14), 4407, doi: 10.1029/2002JD002670
552

553 Riahi, K., et al. (2017): The Shared Socioeconomic Pathways and their energy, land use,
554 and greenhouse gas emissions implications: An overview. *Global Environmental*
555 *Change*, 42, 153-168.
556

557 Rose, B. E. J., Armour, K. C., Battisti, D. S., Feldl, N., & Koll, D. D. B. (2014). The
558 dependence of transient climate sensitivity and radiative feedbacks on the spatial
559 pattern of ocean heat uptake. *Geophysical Research Letters*, 41, 1071–1078.
560 <https://doi.org/10.1002/2013GL058955>.
561

562 Senior, C. A., & Mitchell, J. F. B. (2000): The time-dependency of climate sensitivity.
563 *Geophys. Res. Lett.*, 27, 2685-2688. <https://doi.org/10.1029/2000GL011373>.
564

565 Silvers, L. G., Paynter, D., & Zhao, M. (2018). The diversity of cloud responses to
566 twentieth century sea surface temperatures. *Geophysical Research Letters*, 45, 391–
567 400. <https://doi.org/10.1002/2017GL075583>.
568

569 Stevens, B., Sherwood, S. C., Bony, S., & Webb, M. J. (2016). Prospects for narrowing
570 bounds on Earth’s equilibrium climate sensitivity. *Earth’s Future*, 4(11), 512–522.
571 <https://doi.org/10.1002/2016EF000376>.
572

573 Swart, N. C. and co-authors. (2019). The Canadian Earth System Model version 5
574 (CanESM5.0.3). *Geosci. Model. Dev.*, <https://doi.org/10.5194/gmd-2019-177>.
575

576 Taylor, K. E., Williamson, D., & Zwiers, F. (2000). The sea surface temperature and sea-
577 ice concentration boundary conditions for AMIP II simulations, PCMDI Report No.
578 60, Program for Climate Model Diagnosis and Intercomparison, Lawrence Livermore
579 National Laboratory.
580

581 Williams, K. D., and Coauthors, 2018: The met office global coupled model 3.0 and 3.1
582 (GC3.0 & GC3.1) configurations. *J. Adv. Model Earth Syst.*, 10(2):357–380.
583

584 Winton, M., Takahashi, K. & Held, I. M. (2010): Importance of ocean heat uptake
585 efficacy to transient climate change. *Journal of Climate*, 23, 2333-23444.
586 doi.org/10.1175/2009JCLI3139.1
587

588 Wood, R., and C. S. Bretherton, 2006: On the relationship between stratiform low cloud
589 cover and lower-tropospheric stability. *J. Climate*, 19, 6425–6432.
590

591 Yuan, T., Oreopoulos, L., Platnick, S. E., & Meyer, K. (2018). Observations of local
592 positive low cloud feedback patterns and their role in internal variability and climate
593 sensitivity. *Geophysical Research Letters*, 45, 4438–4445.
594 <https://doi.org/10.1029/2018GL077904>.
595

596 Zhao, M., Golaz, J.-C., Held, I. M., Guo, H., Balaji, V., Benson, R., et al. (2018). The
597 GFDL global atmosphere and land model AM4.0/LM4.0: 1. Simulation
598 characteristics with prescribed SSTs. *Journal of Advances in Modeling Earth
599 Systems*, 10, 691–734. <https://doi.org/10.1002/2017MS001208>.
600

601 Zhou, C., Zelinka, M. D., & Klein, S. A. (2016). Impact of decadal cloud variations on
602 the Earth’s energy budget. *Nature Geoscience*, 9(12), 871–874.
603 <https://doi.org/10.1038/ngeo2828>.
604

605 Zhou, C., Zelinka, M. D., & Klein, S. A. (2017). Analyzing the dependence of global
606 cloud feedback on the spatial pattern of sea surface temperature change with a
607 Green’s function approach. *Journal of Advances in Modeling Earth Systems*, 9,
608 2174–2189. <https://doi.org/10.1002/2017MS001096>.